

# Investigating the electronic and magnetic properties of Dy, Y and La by site substitution on Nd<sub>2</sub>Fe<sub>14</sub>B permanent magnet employing the first-principle approach

LE Miya<sup>a\*</sup>, ME Sithole<sup>a1</sup>, R Modiba<sup>b2</sup>

<sup>a</sup>Department of Physics, Sefako Makgatho Health Science University, P.O. Box 94, Medunsa, 0204, South Africa

<sup>b</sup>Materials Science and Manufacturing, CSIR, P.O. Box 395, Pretoria, 0001, South Africa

Email: l.enerst@gmail.com \*, enoch.sithole@smu.ac.za <sup>1</sup>, rmahlangu1@csir.co.za <sup>2</sup>

## Abstract

The development of new Nd-Fe-B permanent magnets continues to be a pressing matter for the transition to a green economy. Permanent magnets have become significant in applications of highly efficient energy conversion machines and devices. First-principles calculations have been performed by using the density function theory (DFT) within the generalized gradient approximation (GGA) to study the Nd<sub>2</sub>Fe<sub>14</sub>B magnets. The effects of Dy/La/Y on the electronic and magnetic properties of Nd<sub>2</sub>Fe<sub>14</sub>B permanent magnet with the site substitution mechanism were studied. The spin and the orbital magnetic moments of the Nd, Dy, Y, and La ion were found to be opposite to each other, which is in agreement with Hund's rule. Moreover, the total orbital magnetic moment was found to be larger than that of the total spin magnetic moment. Y prefers the 4*f* site, while La on the other hand prefers the 4*g* site. The total magnetic moment of the Nd<sub>2</sub>Fe<sub>14</sub>B was in close agreement with the previous reported experimental value.

**Keywords:** First principle, Permanent magnet, DFT, Nd<sub>2</sub>Fe<sub>14</sub>B, Density of states

## 1. Introduction

Magnetism of solid or condensed matter has for some time been perhaps one of the main issues from both crucial and pragmatic points of view. To this day magnetism remains under immense research activity due to its theoretical complexity and extensive innovative importance (Velu et al. 1988, Coey 2011). Magnetic materials found their applications in permanent magnets, of which these lasting magnets can be classified due to their high magnetocrystalline anisotropy energy (MAE), and strong magnetization. As a result of the capacity of rare-earth (RE) ions to improve the stability of current perpetual magnets against demagnetization fields (coercivity), permanent magnets have a wide scope of mechanical applications, for example, they are segment of wind turbines, huge businesses for engines (electric vehicles engines), attractive reverberation imaging (X-ray) clinical machines, cell phones and significantly more (Buschow 1984, Mitchell 1985). The performance of a permanent magnet can be classified by two fundamental physical quantities, which are the maximum energy product (BH)<sub>max</sub> and coercive field. The maximum energy product (BH)<sub>max</sub> being the energy put away in the magnetic field made by an ideal shaped volume of material, and the coercive field which is the proportion of the stability of a permanent magnet against fields of demagnetization. Studies have been made on various sorts of permanent magnets such as AlNiCo, SmCo<sub>5</sub>, Sm<sub>2</sub>Co<sub>17</sub>, hexagonal ferrites and Nd<sub>2</sub>Fe<sub>14</sub>B (Coey 2014, Sun et al. 2015, Pullar 2012, Al-Omari et al. 2001, Gabay et al. 2008, Croat et al. 1984, Sagawa et al. 1984, Coehoorn 1988). Among the rare-earth (RE) based magnets, Nd<sub>2</sub>Fe<sub>14</sub>B is as yet unrivalled having an interesting combination of high magnetic anisotropy and the best magnetic moments among other permanent magnets (Sagawa et al. 1984, Buschow 1991).

Following the discovery of Nd<sub>2</sub>Fe<sub>14</sub>B, the comprehension of the fundamental basic physical science about the atomic origin of the magnetic anisotropy within the structure is as yet fragmented (Sagawa et al. 1984). Moreover, previous studies make it clear that Nd in the Nd<sub>2</sub>Fe<sub>14</sub>B structure is the most effective rare-earth element with the dominating axial anisotropy, however the viable magnetic moment comes from the Fe atoms (Buschow 1991, Givord et al. 1984, Bogé et al. 1985, Haskel et al. 2005). It is reported that the magnetic anisotropy of Nd on 4*f* site in Nd<sub>2</sub>Fe<sub>14</sub>B is smaller than that on 4*g* site (Alam and Johnson 2014). Studies also confirm that the RE Nd in the Wyckoff sites (4*f* and 4*g* sites) can be possibly supplanted with abundant rare-earth elements (for example La, Ce, Dy) which can lower the expense of the permanent magnet with little traces or negligible usage of Nd in the compound (Alam and Johnson 2014, Herbst et al. 1984). Therefore, if the Nd on 4*f* site is selectively replaced by another RE elements, it very well might be conceivable to grow new Nd-Fe-B type magnet which contains less Nd, without lowering the magnetic properties. Regardless of several reports made, it is not clear how different Wyckoff positions (4*f* and 4*g* site of the RE) in the complex geometry of 2-14-B are responsible in maintaining high magnetocrystalline anisotropy. In addition to the crystalline atomic environment (*g* and *f* in-equivalent sites of the P4<sub>2</sub>/mmn tetragonal space group), isolating the magnetic response emerging just from the Nd ions is troublesome because of the massive magnetic background of Fe ions (Wolfers et al. 1996). The Fe ions are responsible for most of the material's saturation magnetization of 31 as compared to 6 for Nd per formula unit, thus the Fe background make it difficult to interpret the neutron diffraction measurements of nontrivial orientations of the Nd moment, which in turn complicates the overlap of chemical and magnetic diffraction that occurs in ferromagnetic materials (Wolfers et al. 1996, Perdew et al. 1997). In this study,

we investigate the electronic, mechanical and magnetic properties of Dy, Y and La by site substitution mechanism (Wyckoff positions *4f* and *4g*) on Nd<sub>2</sub>Fe<sub>14</sub>B permanent magnet employing the first-principles approach.

## 2. Method

We performed spin-polarized calculations without spin-orbital interaction using the density functional theory (DFT) in the generalized gradient (GGA), with the Perdew-Burke-Ernzerhof (PBE) function for exchange-correlation potential employed in Cambridge Sequence Total Energy Package (CASTEP) to study the electronic, mechanical, and magnetic properties of 2-14-B type compound (Payne et al. 1992, Clark et al. 2005, Kresse and Joubert 1999). In this study, our focus is to investigate the effects of doping process on two non-equivalent sites RE(*4f*) and RE(*4g*) Wyckoff positions with the Dy/La/Y atoms in order to reduce the Nd (critically) usage in the compound. Projector augmented-wave (PAW) potentials have been employed to illustrate the electron-ion interaction (Monkhorst and Pack 1976). To obtain the ground state optimization, we have utilized the Broyden-Fletcher-Goldfarb-Shanno (BFGS) minimization technique. The convergence criterion for structure optimization and energy calculations were set to fine quality with the tolerance for the stress concentration factor (SCF), energy, maximum force and maximum displacement set to eV/atom, eV/atom, 0.03 eV/Å, and 0.001Å respectively for all calculations. An energy cutoff of 500 eV was set and the Monkhorst-Pack k-point grids of 3×3×2 have been applied for the Brillouin-zone (BZ) integration Pack (Monkhorst and Pack 1976). To correctly account for the magnetic properties due to the effects of Dy, Y and La on magnetic systems, spin-polarization was included using formal spin as initial in the calculations.

## 3. Results and discussion

### 3.1 Structural and magnetic properties of R<sub>2</sub>Fe<sub>14</sub>B

In this section the structural and magnetic properties of R<sub>2</sub>Fe<sub>14</sub>B (R = Nd, Dy, Y and La) tetragonal structure composed of 68 atoms (i.e., 4B, 8Nd and 56Fe atom arranged in an eight-layer structure) unit cell and a space group of *P4<sub>2</sub>/mmm* are discussed. The RE

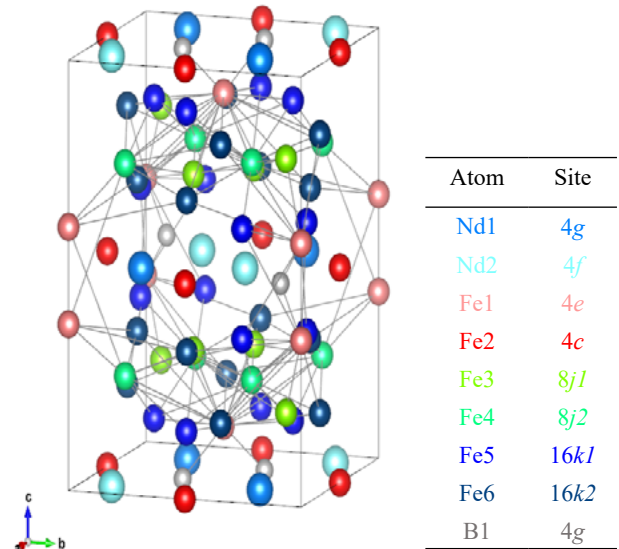


**Figure 1:** The crystal structure of Nd<sub>2</sub>Fe<sub>14</sub>B

atoms occupy two distinct crystallographic site the R(*f*) and R(*g*), and the Fe atoms occupy six non-equivalent sites the *e*, *c*, *j1*, *j2*, *k1* and *k2*. Figure 1 shows structure of Nd<sub>2</sub>Fe<sub>14</sub>B.

In Table 1 & 2, the structural and magnetic properties of the R<sub>2</sub>Fe<sub>14</sub>B structures are shown wherein all the structures were subjected to full geometry optimization to find their ground states. The pseudo-atomic configuration adopted is 4f<sup>4</sup> 5s<sup>2</sup> 5p<sup>6</sup> 6s<sup>2</sup>, 3d<sup>6</sup> 4s<sup>2</sup> and 2s<sup>2</sup>, for Nd, Fe and B, respectively. The optimised lattice parameters for Nd, Dy, Y and La structures are shown in Table 1, respectively. The *c/a* ratio with respect to the Nd, Dy, Y and La is 1.369, 1.353, 1.362 and 1.4, the *c/a* ratio is increased by the tetragonal distortion of the crystal structure. The calculated magnetic moment  $M_s(\mu_B)$  of Fe sites of Nd, Dy, Y and La structures are shown in Figure 2. These Fe site magnetic moments are in good agreement with other two reported results obtained from neutron-scattering experiments, one on power samples and the other on single crystals (Sagawa et al. 1984, Burzo 1998). The recursion method and a semi-tight binding were used, and they yielded the largest magnetic moment of the Fe atoms at the *j2* site. Moreover, using the spin-polarized

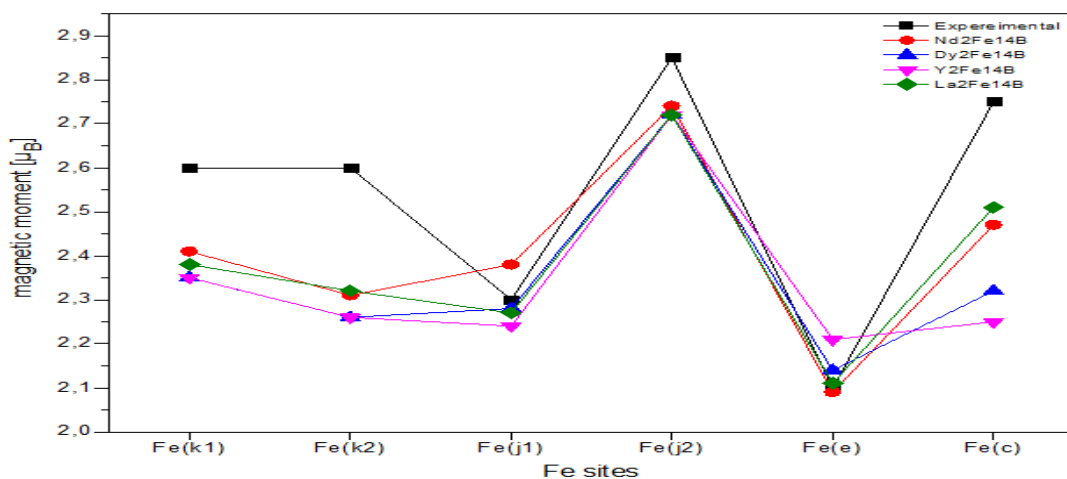


**Figure 2:** Total calculated magnetic moments of Fe sites of R<sub>2</sub>Fe<sub>14</sub>B structure in units per atom. Filled black squares, red circles, blue triangles(up), pink triangles(down) and green diamonds indicate Experimental Fe sites of Nd<sub>2</sub>Fe<sub>14</sub>B, Nd<sub>2</sub>Fe<sub>14</sub>B, Dy<sub>2</sub>Fe<sub>14</sub>B, Y<sub>2</sub>Fe<sub>14</sub>B and La<sub>2</sub>Fe<sub>14</sub>B.

only, we obtained the largest magnetic moment of Fe at  $j2$ , but the smallest magnetic moment of Fe was found at  $e$ , which both have the same local symmetry but are located at different environments, thus this suggest that there are some Fe sites that drive the rest into a magnetic state and that themselves too can acquire the largest moments. The Fe atom at  $j2$  is bonded to four other Fe atoms at the sites  $kl$ ,  $k2$ ,  $jl$  and  $e$ , whilst the Fe atom at site  $e$  is bonded to three Fe atomic sites, that is, the  $kl$ ,  $k2$  and  $jl$ , and one B site at  $g$ . The site-decomposed magnetic moments at different Fe sites of R<sub>2</sub>Fe<sub>14</sub>B (R = Nd, Dy, Y, La) are summarized in Table 2 below. The hybridization between the RE and Fe atoms fundamentally rely upon the distance between the RE and Fe atoms within the crystal structure. In addition, it is widely known that the total spin magnetic moment of the Fe atoms is parallel to that of the Nd atoms at the  $4f$  site. The ferromagnetic alignment of the Nd and Fe moments is due to the parallel alignment favoured between the hybridization of the Fe  $3d$  states and the Nd  $5d$  states, as well as the fact that the total  $4f$  magnetic moment is in the opposite direction of the total  $4f$  spin moment and the  $4f$  and  $5d$  spins are parallel on the Nd atom. The Dy<sub>2</sub>Fe<sub>14</sub>B is in a ferrimagnetic alignment. Figure 2 shows the calculated magnetic moments of Fe sites of R<sub>2</sub>Fe<sub>14</sub>B in  $\mu_B$  units per atom.

**Table 1:** Lattice parameters (Å) of R<sub>2</sub>Fe<sub>14</sub>B

| Structure                          | $a$   | $c$    | $c/a$ |
|------------------------------------|-------|--------|-------|
| Nd <sub>2</sub> Fe <sub>14</sub> B | 8.813 | 12.063 | 1.369 |
| Dy <sub>2</sub> Fe <sub>14</sub> B | 8.768 | 11.864 | 1.353 |
| Y <sub>2</sub> Fe <sub>14</sub> B  | 8.738 | 11.904 | 1.362 |
| La <sub>2</sub> Fe <sub>14</sub> B | 8.810 | 12.334 | 1.4   |

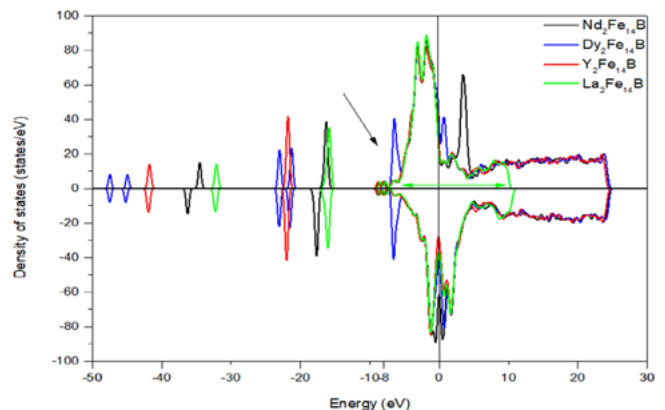
**Table 2:** The site-decomposed magnetic moments at different Fe sites Bohr magneton ( $\mu_B$ ) of R<sub>2</sub>Fe<sub>14</sub>B

| Fe sites   | Nd   | Dy   | Y    | La   | Ex   |
|------------|------|------|------|------|------|
| Fe( $kl$ ) | 2.41 | 2.35 | 2.35 | 2.38 | 2.60 |
| Fe( $k2$ ) | 2.31 | 2.26 | 2.26 | 2.32 | 2.60 |
| Fe( $jl$ ) | 2.38 | 2.28 | 2.24 | 2.27 | 2.30 |
| Fe( $j2$ ) | 2.74 | 2.72 | 2.72 | 2.72 | 2.85 |
| Fe( $e$ )  | 2.09 | 2.14 | 2.21 | 2.11 | 2.10 |
| Fe( $c$ )  | 2.49 | 2.32 | 2.25 | 2.51 | 2.75 |

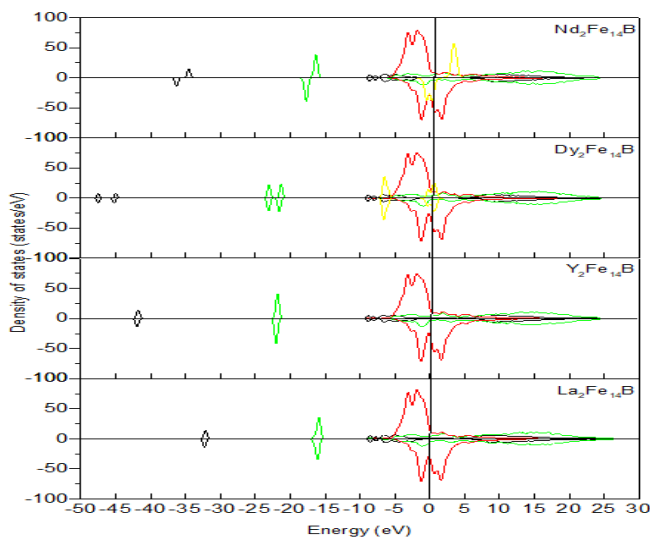
### 3.2 Density of States (DOS)

Figure 3 shows the density of states (DOS) of the R<sub>2</sub>Fe<sub>14</sub>B (R = Nd, Dy, Y, La) structures, which were performed based on spin-polarized calculations without including spin-orbit coupling and observed the exchange splitting of the higher and lower energy regions separated by the Fermi level ( $E_f$ ). The DOS generates the number of electronic states per unit energy interval. The spin (up-down) and the partial DOS of the R<sub>2</sub>Fe<sub>14</sub>B crystal structure are shown in Figure (3&4). The Fe in the  $3d$ -states represented by the valley due to the two peaks is dominant in the total spin-up (alpha) DOS for R<sub>2</sub>Fe<sub>14</sub>B, with localized peaks between -5 to 25 eV for all the Nd, Dy and Y structures. With of course, the exception of the La<sub>2</sub>Fe<sub>14</sub>B which is between -5 to 10 eV, though within the previously mentioned range, as shown in Figure 3. The bandwidth of the Fe  $d$ -states in La<sub>2</sub>Fe<sub>14</sub>B is shorter than that of the Nd, Dy and Y structures because the lattice parameter of La<sub>2</sub>Fe<sub>14</sub>B was greater

than all the other structures. While the clustered peaks around the  $E_f$  represent the highly localized Nd for both  $4f$  and  $4g$  sites and the low peaks at -8 are due to the hybridization between B- $2s$  and B- $2p$  states with the Fe- $4s$  and Fe- $4p$  states as shown in Figure (3&4), of which these  $2s$  states bring a small amount of Fe states down to this region. The likely Fe states that will be brought down to this region are the  $kl$  and  $e$  Fe sites, which are the closest to the B atoms within the crystal structure. On the other hand, the Fe in the  $3d$  states peaks in Figure (3) are also responsible for dominating the total spin-down (beta) DOS from -3 to 3 eV. Also, the highly localized peaks for Nd at  $4f$  and  $4g$  are found to be above the  $E_f$  as shown in Figure (3) and the two low peaks located from -7 to 8 eV are due to the B states as shown in Figure (3). The major peak of spin-up (alpha) is at the  $j2$  site, just below the  $E_p$ , whereas most of the spin-down is above the  $E_p$ , thus resulting in a large spin magnetic moment. The notable differences in the PDOS graphs are due to strong different local environments at Fe sites and the distance between the RE and the Fe atoms, which strongly affect the difference between states of the Nd, Dy, Y and La atoms in the crystal structure. Despite the semi-core treatment of  $4f$  and  $4g$  sites, the magnetic moments of the Fe atoms do reflect the difference in states of the Nd, Dy, Y and La atoms. The PDOS graphs are similar, with major peaks at about 3 eV below the  $E_f$  with no prominent structures elsewhere. The similar trend in the PDOS of different structures is a strong indication of the influence of the crystalline anisotropy in the Fe sublattice on the electronic structure. The magnetic moments of both the Nd and the B sites are in the opposite direction to the Fe magnetic moments. In addition, we found anti-parallel spins and magnetic moments on the Nd sites. Which is in agreement with the Hund's rule that the total magnetic moment of the RE ion and its spin moment are anti-parallel to each other for light lanthanides (Herbst 1991). Also, the total orbital magnetic moment obtained was larger than the spin magnetic moment. With regard to the charge transfers, they are found to be small, ranging between 1.8 and -0.05, which is expected for calculations for metallic states with reasonable choices of atomic spheres. Using the spin-polarized only we calculated the total magnetic moment of Nd<sub>2</sub>Fe<sub>14</sub>B was 39.8  $\mu_B$ , which is larger, as compared to the experimental value of 35.0  $\mu_B$ /f.u. or 37.1  $\mu_B$ /f.u. (Sagawa et al. 1984, Burzo 1998). The calculated magnetic moment of Dy<sub>2</sub>Fe<sub>14</sub>B, Y<sub>2</sub>Fe<sub>14</sub>B and La<sub>2</sub>Fe<sub>14</sub>B are 12.6, 29.9, 30.5  $\mu_B$ /f.u., respectively. The calculated magnetic



**Figure 3:** Comparison of the total density of states (tDOS) for R<sub>2</sub>Fe<sub>14</sub>B (R = Nd, Dy, Y, La) structures. The Fermi energy is taken as the energy zero ( $E = E_f = 0$ )



**Figure 4:** Comparison of the partial density of states (PDOS) for  $R_2Fe_{14}B$  ( $R = Nd, Dy, Y, La$ ) structures. The lines in different colours (black, green, red, yellow) represents the  $s, p, d, f$  states respectively. The Fermi energy is taken as the energy zero ( $E = E_F = 0$ )

moments were in good agreement with previous theoretical work and experimental data. The calculations of the magnetic moments can be improved with full relativistic treatment.

#### 4. Conclusions

In this study, the magnetic properties of  $R_2Fe_{14}B$  using ab-initio techniques have been explored. Using spin-polarized only we found the magnetic moments of Fe sites to be in the opposite direction to the magnetic moments of both the Nd and the B sites. In addition, we found anti-parallel spins and magnetic moments on the Nd sites. Which is in agreement with the Hund's rule on lanthanides, that the total magnetic moment of the RE ion and its spin moment are anti-parallel to each other for light lanthanides (Herbst 1991). Moreover, it was observed that in all the structures, the total orbital magnetic moment was larger than that of the total spin magnetic moment. In addition, Y prefers the  $4f$  site, while La on the other hand prefers the  $4g$  site. The total magnetic moment of the  $Nd_2Fe_{14}B$ ,  $Dy_2Fe_{14}B$ ,  $Y_2Fe_{14}B$  and  $La_2Fe_{14}B$  were in close agreement with the previous reported experimental value. The findings of this study are the 1<sup>st</sup> step of the ingoing future work towards green economy.

#### Acknowledgements

The authors acknowledge the CSIR for their financial support. The calculations were conducted using computer resources at the Centre for High Performance Computing (CHPC) in Cape Town.

#### References

- Alam, A., Johnson, D.D., 2014. Mixed valency and site-preference chemistry for cerium and its compounds: A predictive density-functional theory study. *Physical Review B*, 89, 235126.
- Al-Omari, I.A., Skomski, R., Thomas, R.A., Leslie-Pelecky, D., Sellmyer, D.J., 2001. High-temperature magnetic properties of

- mechanically alloyed  $SmCo_5$  and  $YCo_5$  magnets. *IEEE transactions on magnetics*, 37, 2534-2536.
- Bogé, M., Coey, J.M.D., Czjzek, G., Givord, D., Jeandey, C., Li, H.S., Oddou, J.L., 1985.  $3d-4f$  magnetic interactions and crystalline electric field in the  $R_2Fe_{14}B$  compounds: Magnetization measurements and Mössbauer study of  $Gd_2Fe_{14}B$ . *Solid state communications*, 55, 295-298.
- Burzo, E., 1998. Permanent magnets based on R-Fe-B and R-Fe-C alloys. *Reports on Progress in Physics*, 61, 1099.
- Buschow, K.H.J., 1984. *Handbook on the Physics and Chemistry of Rare Earth*, 6. North-Holland, Amsterdam: edited by Gschneidner, K.A. Jr., and Eyring, L.
- Buschow, K.H.J., 1991. New developments in hard magnetic materials. *Reports on Progress in Physics*, 54, 11-23.
- Clark, S.J., Segall, M.D., Pickard, C.J., Hasnip, P.J., Probert, M.I., Refson, K., Payne, M.C. 2005. First principles methods using CASTEP. *Zeitschrift für kristallographie-crystalline materials*, 220, 567-570.
- Coehoorn, R., De Mooij, D.B., Duchateau, J.P.W.B. and Buschow, K.H.J., 1988. Novel permanent magnetic materials made by rapid quenching. *Le Journal De Physique Colloques*, 49, 669-670.
- Coey, J.M.D., 2011. A perspective. *IEEE Transactions on magnetics. Hard magnetic materials*, 47, 4671-4681.
- Coey, J.M.D., 2014. New permanent magnets; manganese compounds. *Journal of Physics: Condensed Matter*, 26, 200-211.
- Croat, J.J., Herbst, J.F., Lee, R.W., Pinkerton, F.E., 1984. Pr-Fe and Nd-Fe-based materials: A new class of high-performance permanent magnets. *Journal of Applied Physics*, 55, 2078-2082.
- Gabay, A.M., Marinescu, M., Liu, J., Hadjipanayis, G.C., 2008. Sintered  $Sm_2Co_7$  Based Magnets with Small Additions of Indium. *IEEE Transactions on Magnetism*, 44, 4218-4221.
- Givord, D., Li, H.S., Perrier de la Bthie, R., 1984. *Solid State Communiqué*, 51, 857.
- Haskel, D., Lang, J.C., Islam, Z., Cady, A., Srajer, G., Van Veenendaal, M., Canfield, P.C., 2005. Atomic origin of magnetocrystalline anisotropy in  $Nd_2Fe_{14}B$ . *Physical review letters*, 95, 207-217.
- Herbst, J.F., 1991.  $R_2Fe_{14}B$  materials: Intrinsic properties and technological aspects. *Reviews of Modern Physics*, 63, 819.
- Herbst, J.F., Croat, J.J., Pinkerton, F.E., Yelon, W.B., 1984. Relationships between crystal structure and magnetic properties in  $Nd_2Fe_{14}B$ . *Physical Review B*, 29, 4176.
- Kresse, G., Joubert, D., 1999. Self-interaction correction to density-functional approximations for many-electron systems. *Physics Review B; Condensed Matter*, 59, 1758-1775.
- Mitchell, I.V., 1985. *Nd-Fe permanent magnets: their present and future applications*. London and New York.
- Monkhorst, H.J., Pack, J.D., 1976. Special points for Brillouin-zone integrations. *Physical review B*, 13, 5188.
- Payne, M.C., Teter, M.P., Allan, D.C., Arias, T.A., Joannopoulos, A.J., 1992. Iterative minimization techniques for ab initio total-energy calculations: molecular dynamics and conjugate gradients. *Reviews of modern physics*, 64, 1045.
- Perdew, J.P., Burke, K., Ernzerhof, M., 1997. Generalized gradient approximation made simple. *Physical review letters*, 78, 1396-1397.
- Pullar, R.C., 2012. Hexagonal ferrites: a review of the synthesis, properties, and applications of hexaferrite ceramics. *Progress in Materials Science*, 57, 1191-1334.
- Sagawa, M., Fujimura, S., Togawa, N., Yamamoto, H., Matsuura, Y., 1984a. New material for permanent magnets on a base of Nd and Fe. *Journal of Applied Physics*, 55, 2083-2087.
- Sagawa, M., Fujimura, S., Yamamoto, H., Matsuura, Y., Hiraga, K., 1984b. Permanent magnet materials based on the rare earth-iron-boron tetragonal compounds. *IEEE transactions on Magnetism*, 20, 1584-1589.
- Sun, Y.L., Zhao, J.T., Liu, Z., Xia, W.X., Zhu, S.M., Lee, D., Yan, A.R., 2015. The phase and microstructure analysis of Alnico magnets with high coercivity. *Journal of Magnetism and Magnetic Materials*, 379, 58-62.
- Velu, E., Dupas, C., Renard, D., Renard, J.P., Seiden, J., 1988. Enhanced magnetoresistance of ultrathin multilayers with perpendicular anisotropy. *Physical Review B*, 37, 668.
- Wolfers, P., Obbade, S., Fruchart, D., Verhoef, R., 1996. Precise crystal and magnetic structure determinations. Part I: a neutron diffraction study of  $Nd_2Fe_{14}B$  at 20K. *Journal of alloys and compounds*, 242, 74-79.